

Available online at www.sciencedirect.com

SCIENCE @ DIRECT®

Applied Surface Science xxx (2005) xxx–xxx

applied
surface sciencewww.elsevier.com/locate/apsusc

Scanning probe microscopy studies of PbS surfaces oxidized in air and etched in aqueous acid solutions

Yuri L. Mikhlin*, Alexander S. Romanchenko, Alexander A. Shagaev

Institute of Chemistry and Chemical Technology SB RAS, K. Marx Street, 42, Krasnoyarsk 660049, Russia

Received 10 February 2005; received in revised form 9 July 2005; accepted 9 July 2005

Abstract

Natural n-type PbS single crystals have been studied using AFM, STM and STS after long-term oxidation in air at ambient temperatures and extensive etching in aqueous acid solutions, in contrast to previous work devoted to initial corrosion of fresh surfaces. The exposure of PbS to atmosphere at high relative humidity for several days yields widespread loose oxidation products; the process is much slower at low humidity. Surface morphologies diverge after the treatment in 1 M perchloric and hydrochloric acid solutions at room temperature and become widely different at elevated temperatures, displaying commonly etch pits up to several micrometers in size and depth along with rather uniformly distributed 20–100 nm protrusions of PbS phase. The changes both in topography and semiconducting properties of PbS found by tunneling spectroscopy have been explained in terms of the non-uniform distribution of donor- and acceptor-type defects D^+/D^- in the metal depleted surface layer, which are generated by chemical reactions and, in turn, determine the rates of the PbS corrosion. In particular, the D^- centers exhibit a self-catalyzing effect on the non-oxidative local dissolution of PbS in HCl media, resulting in the deep etch pits. © 2005 Elsevier B.V. All rights reserved.

Keywords: Lead sulfide; Oxidation; Acidic dissolution; Scanning probe microscopy; Tunneling spectroscopy; Surface topography

1. Introduction

Lead sulfide (PbS, galena) is the major ore mineral of lead and is applied in infrared detectors as a semiconductor with the band gap of about 0.4 eV [1,2]. Furthermore, PbS nanoparticles attract much attention due to strong confinement effects on electrons and phonons [2]. The surface characteristics and reaction

mechanisms for PbS oxidation in air and aqueous solutions are important for mineral processing, geochemistry, and the production, performance and degradation of optoelectronic devices. Conditioning in aqueous acidic solutions represents a standard etching procedure for II–VI and IV–VI semiconductors and a prospective process of hydrometallurgical recovery of lead. Consequently, lead sulfide surfaces have been extensively studied in order to understand their composition, structure and properties, to specify products and to gain an insight into the reaction mechanisms (see, e.g., [1,3–8] and references herein).

* Corresponding author. Tel.: +7 3912 494885; fax: +7 3912 238658.

E-mail address: yumikh@icct.ru (Y.L. Mikhlin).

Apart from elemental sulfur and oxygen-containing compounds of lead and sulfur (PbO , Pb(OH)_2 , PbSO_4 , etc.), X-ray photoelectron spectroscopy (XPS) examination of a variety of reacted surfaces revealed considerable depletion of the sulfidic phase in metal due to more rapid release of Pb during PbS interaction with air and aqueous solutions [4,8–14]. It was also found that PbS reactivity strongly depends on anionic composition of acid solutions [12,13]. Basing on XPS, X-ray spectroscopy, scanning electron microscopy (SEM), dissolution kinetics and electrochemistry studies, we have proposed recently [8,12,13] to describe such non-stoichiometric disordered layers of PbS and other metal sulfides in much the same way as non-crystalline semiconducting chalcogenides, which special properties are thought to be due to the presence and non-uniform distribution of plentiful defects having negative correlation energy (Hubbard energy) [15,16].

A number of researchers employed scanning probe microscopy (SPM) to examine PbS surfaces [17–32]. Eggleston and Hochella [17–21] found using scanning tunneling microscopy (STM) and tunneling spectroscopy (STS) that PbS oxidation in air and under oil is non-uniform and probably autocatalytic, showing a decreased brightness of S sites in areas with [1 1 0]-parallel borders. Tunneling spectra taken in air were indicative of the gap width of about 0.25 eV and n-type conductivity of the semiconductor surface [18–20]; they are dissimilar to calculated spectra [22–24]. Several STM studies in air [25,26] and aqueous systems [27,28] showed the protrusions composed of oxidation products, which were randomly scattered on natural galena but were preferentially located on terrace steps at synthetic specimens, suggesting that the oxidation starts at impurities and crystal defects. Wittstock et al. [29] observed using in situ atomic force microscopy (AFM) a roughening of the surface ascribed to non-oxidative galena dissolution in acetate buffer (pH 4.9) and then, at anodic potentials, two types of protrusions formed by sulfur, which differed in the size and mutual distances. Higgins and Hamers found by in situ STM that both electrochemical oxidation and reduction in oxygen-depleted perchlorate solutions (pH 1.7) [30], and acidic dissolution of galena in sulfate media (pH 2.7 and 7) [31] proceed via removal of material from step edge and are fastest along the [1 0 0] directions. Moreover, impurity-related defects were considered to entail etch pit development at terraces under oxidizing

conditions. De Giudici and Zuddas [32] performed an in situ AFM investigation of galena dissolution in air-saturated HCl solutions (pH 1 and 3) over 45 h. Square etch pits reached a depth of 80 nm in first hours, and then nucleation and growth of new etch pits was inhibited, possibly due to homogeneously distributed protrusions 1–3 nm high, so large rough terraces delimited by macrosteps 50–100 nm high were formed. The authors concluded that the protrusions were composed of elemental sulfur, the dissolution of which (as oxysulfur anions) represents the rate-limiting step of the overall process. Most recently, Cama et al. [33] reported the results of non-stirred flow-through kinetics experiments, in situ and ex situ AFM, and XPS surface analysis of galena reacted in hydrochloric acid solutions (pH 1–3) at 20–25 °C, which agreed with the dissolution mechanisms suggested in Ref. [32]. Furthermore, the ex situ tapping mode images show the growth of larger protrusions of sulfur and lead sulfate on galena substrate at acidic pH, particularly in more oxidative media containing HNO_3 instead HCl or Fe^{3+} ions.

It is worth emphasizing that the chemical reactions were conducted at room temperature in all the SPM studies cited above, and they mostly dealt with initial stages of PbS corrosion. There is a need, however, to understand longer-term metal sulfide corrosion rather than just initial corrosion of fresh surfaces. In the current paper, we report scanning probe microscopic images and tunneling spectra of natural PbS single crystal surfaces oxidized in air for long periods or substantially modified in aqueous acidic solutions. The images were recorded ex situ in order to conduct the chemical treatment under fairly severe conditions. The acidic etching was found to pattern the reacted surfaces simultaneously in nano- and micrometer scales and to modify semiconducting characteristics, differently in various solutions. These results shed new light on mechanisms of the metal sulfide reactivity and open up possibilities for creation of premeditated surface topographies.

2. Experimental

Single crystals of natural galena obtained from Geological Museum of Central Siberia had less than 0.1% by mass of metal impurities and no inclusions of

other phases. The material was of n-type conductivity with $(1-10) \times 10^{17} \text{ cm}^{-3}$ electron density determined from Hall effect measurements. Galena samples of about $4 \text{ mm} \times 3 \text{ mm} \times 1 \text{ mm}$ were prepared from the mineral lumps by cleavage in air to obtain a flat PbS (1 0 0) surface. The samples were exposed to laboratory atmosphere or were stored in a desiccator (with periodical access for laboratory air) at $20 \pm 3 \text{ }^\circ\text{C}$ above an aqueous ammonium sulfate solution, which provides about 90% relative humidity (RH), and were examined by SPM at predetermined times up to 12 months. Alternatively, the specimens after the cleavage were conditioned in 1 M acid solutions in a water-jacket glass vessel without agitation at $\pm 1 \text{ }^\circ\text{C}$ controlled temperature. Usually, no attempt was made to prevent ingress of air and to flush H_2S produced but in some cases argon was used to purge oxygen from solutions before the experiment. In several experiments, the single crystals were treated together with galena powdered to about $60 \text{ }\mu\text{m}$ grain size (0.3 g) in order to reduce the electrochemical potential of the media. Reagent grade chemicals and doubly distilled water were used to prepare solutions. After the etching, the specimen was quickly rinsed with water and allowed to desiccate in the atmosphere before the SPM examination.

AFM, STM and STS investigations were performed at the same specimens using a multimode Solver P47 device equipped with a $14 \text{ }\mu\text{m}$ scanner (NT-MDT, Russia) at ambient conditions. No less than three points at each of at least three to four galena samples treated in parallel were imaged. The AFM experiments were conducted mainly in the tapping mode, with the height and phase shift images recorded simultaneously; the resonant frequency of vibration of the silicon cantilever was in the range 150–250 kHz. Some tests carried out in the contact mode (constant deflection regime, the cantilever force constant of 0.05 N/m) displayed very similar results. The tips used in STM and STS measurements were mechanically cut 90% Pt–10% Ir wires. Typical STM bias voltage and tunneling current were -0.1 V and 0.1 nA , respectively; positive bias was defined as a positive voltage on the sample with respect to the tip. AFM and STM images were collected at the scan rate of 1–2 Hz with 512 lines per scan; no smoothing procedure was applied. To exclude the possibility of dirty-tip and multi-tip artifacts, scan angle was rotated during image collection. Although quite reproducible, the STM images were often of poor

quality due to occurrence of low-conducting oxidation products and complex PbS topography, so only few of them are shown in following figures. The $I-V$ and $dI/dV-V$ curves were measured using a fixed tip-sample separation by breaking the feedback circuit for a few microseconds at a desired surface location. All curves given in this paper represent the average over approximately 10 measurements without changing the lateral position, the tip-sample distance and the potential sweep rate. They were reproduced in a series of locations over the sample; the influence of the local characteristics for heterogeneous surfaces is discussed below.

3. Results

3.1. Cleaved and air-oxidized PbS surfaces

Fig. 1 shows AFM images of typical cleaved PbS surfaces. Fresh surfaces are characterized by large, almost atomically flat [0 0 1] terraces between atomic steps of 0.3 nm to several hundreds nanometers in height, which mainly are parallel to $\langle 100 \rangle$ and equivalent crystallographic directions.

AFM exhibits some roughening of the terraces, and STM images become noisier over the aerial oxidation. Significant changes in the topography occur at high RH after 1–2 days exposure when protrusions 20–100 nm

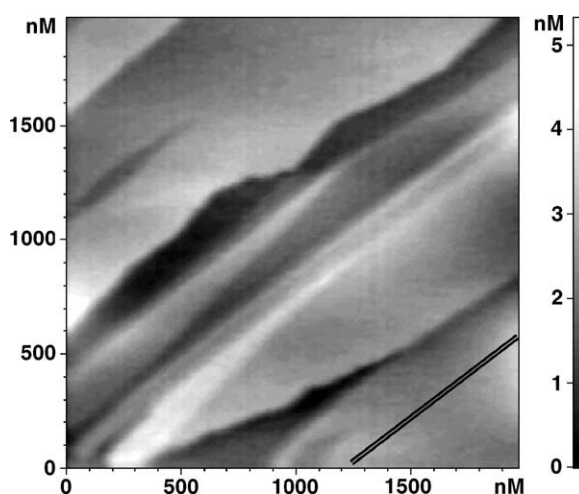


Fig. 1. Tapping mode AFM images of a typical fresh cleavage surface of PbS. Double line indicates direction parallel to $\langle 100 \rangle$.

in diameter and 5–15 nm in height arise first at certain several micrometer sized areas, and they cover the entire surface over 3–5 days (Fig. 2). The protrusions are detectable both in the tapping and contact AFM modes, but STM displays only their marks on a noisy background. The material making up the protrusions is loose and can be easily moved by a cantilever impact (Fig. 2a); they coalesce producing up to a few micrometers large piles and thin irregular coatings after 7–10 days. The oxidation is much slower and, aside from a small roughening, noticeable products appear on the galena surfaces in laboratory air with 40–60% RH after the exposure times of 2–3 weeks. The PbS ageing for several months results in irregular surfaces exhibiting a nanometer-scale roughness, pits few nanometers deep and 30–100 nm in diameter, and accumulations of the solid products (Fig. 2b). For samples exposed to the laboratory air with RH varied from 60 to 100% for several summer months (Fig. 2c), typical are submicrometer-wide tracks formed probably by microdrops of condensed water, which runs transferred the covering products.

Rinsing of the oxidized specimens with water removes most of the oxidation products, but leaves nanometer-scale traces of the accumulations (not shown in figures). All the products actually are not observable in STM images, which are clearer than those from the samples exposed to the humid atmosphere for several days but are still noisy. Previous works [3–13,18–22] have shown that the oxidation products that accumulate on PbS surface under similar conditions are composed of elemental sulfur, lead oxide, lead hydroxide and, in lesser amounts, lead sulfates and carbonates. Water adsorbed and condensed on the surface promotes the PbS oxidation and then wets and renders the product morphology. It is also evident that the PbS corrosion begins with and is localized to a considerable degree in spatial spots, which are randomly scattered or, if the oxidation rate is fast enough as in the humid air, quite uniformly distributed over the surface.

3.2. PbS surfaces etched in perchloric acid solutions

Initial stages of the PbS etching in 1 M HClO₄ (in particular, at room temperature during 10 min) produce steps oriented largely along the equivalent

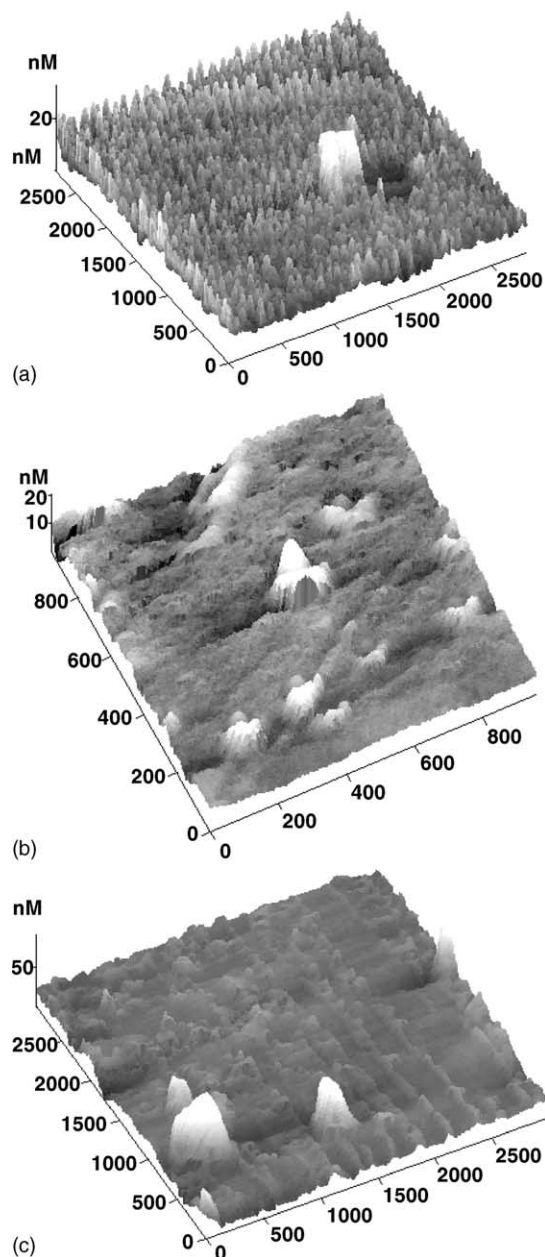


Fig. 2. Three-dimensional AFM images of air-oxidized PbS. (a) Contact mode image of the PbS surface exposed to the atmosphere (RH 90%) for 3 days. A heap formed by the products shifted by the cantilever and a fracture step (in the right top corner of the image) are seen. Tapping mode images (b and c) of the PbS surfaces aged in the laboratory air for 6 months. The figure (b) illustrates the formation of pits and product accumulations on the oxidized surfaces. In figure (c), tracks nearly parallel to the image borders are produced by submicrodrops of condensed water.

[1 1 0] directions (Fig. 3a), in consistence with in situ STM images observed after PbS immersion in sulfate solution (pH 2.7) for 20 min [31], although the steps are mainly 0.6–0.7 nm in height, corresponding to two atomic layers (0.64 nm) but not monatomic. In addition, a number of small protrusions about 2 nm in height and 10 nm in length, similar to the features visible at the in situ STM images [31], seem to

represent some PbS spots which dissolve much slower. After more prolonged etching at the ambient temperature, AFM usually detects nearly flat top protrusions about 5 nm high, ranging in size from several nanometers to hundreds nanometers (Fig. 3b); these details are widespread if the sample has been exposed to atmosphere for a period of several days or longer. The surface images recorded using STM are similar but noisy. This implies that the surface topography is unlikely due to accumulation of insoluble reaction products, and we therefore propose that the surface topography is comprised of different types of surface that dissolve at distinct rates.

More intensive PbS dissolution eliminates steps and other intrinsic defects and confines the protrusion size within 20–80 nm. After the PbS etching at 50 °C for 1 h (Fig. 4), the round-shape protrusions completely cover the surface and their heights increase, displaying rather narrow distribution ranged 20–70 nm. These features display small contrast in the phase imaging AFM (Fig. 4a') and are seen in STM, indicating that they are formed by PbS projections yet again. The height histograms obtained from a tapping mode AFM image and an STM one (Fig. 4b) have the same maximum value but the former is wider and asymmetric possibly due to a finite radius of the cantilever tip. Alternatively, this discrepancy may be explained by a presence of elemental sulfur or other products undetectable by STM. Such species can be observed using large-scale AFM scans (Fig. 4c), which also show that, in addition to the protrusions, the surface relief consists of valleys several micrometers in length but only a few hundred nanometers deep, with rather gentle side-wall slopes bounded by relatively sharp ridges. As the etching time increases to 2–3 h, the protrusions grow somewhat, whereas the valleys reduce in area but become deeper.

3.3. PbS etched in hydrochloric acid solutions

PbS surfaces contacted with 1 M HCl at room temperature for 10–20 min become covered by 1–5 nm high protrusions up to 100 nm in diameter, having crater-like tops, and square and rounded pits less 50 nm deep (Fig. 5a). The etch pits randomly disperse at terraces for the majority of samples, but in few occasions the pits are concentrated along the steps parallel to [0 0 1] or equivalent directions.

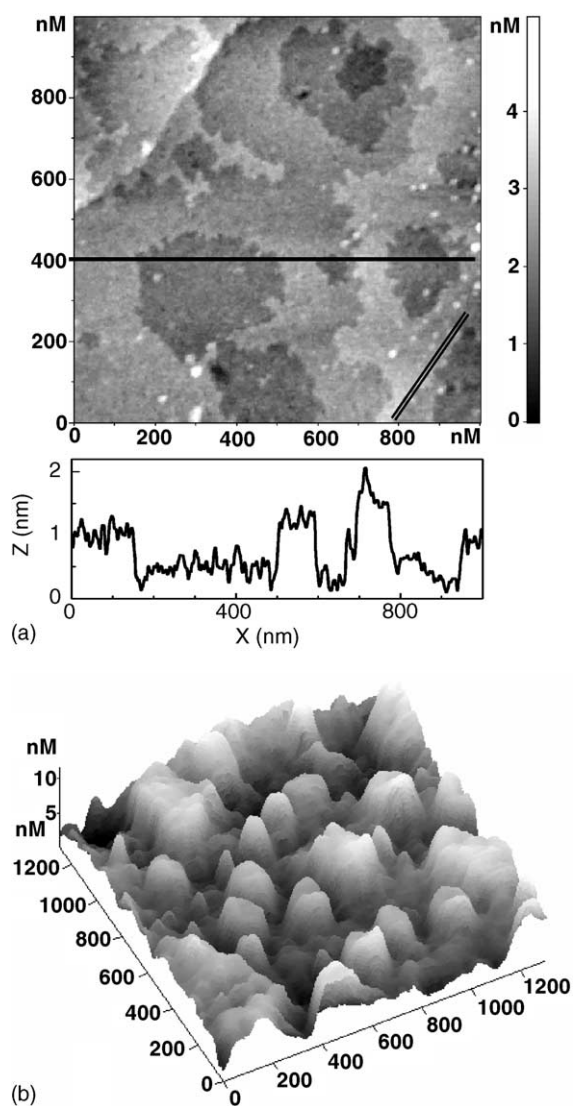


Fig. 3. (a) STM ($I = 0.1$ nA, $V = -0.1$ V) and (b) AFM images of a PbS crystal etched in 1 M HClO_4 at 20 °C for (a) 10 min and (b) 30 min. Cross-sectional profile is shown for the image (a) at $y = 400$ nm. Double line indicates direction parallel to $\langle 100 \rangle$.

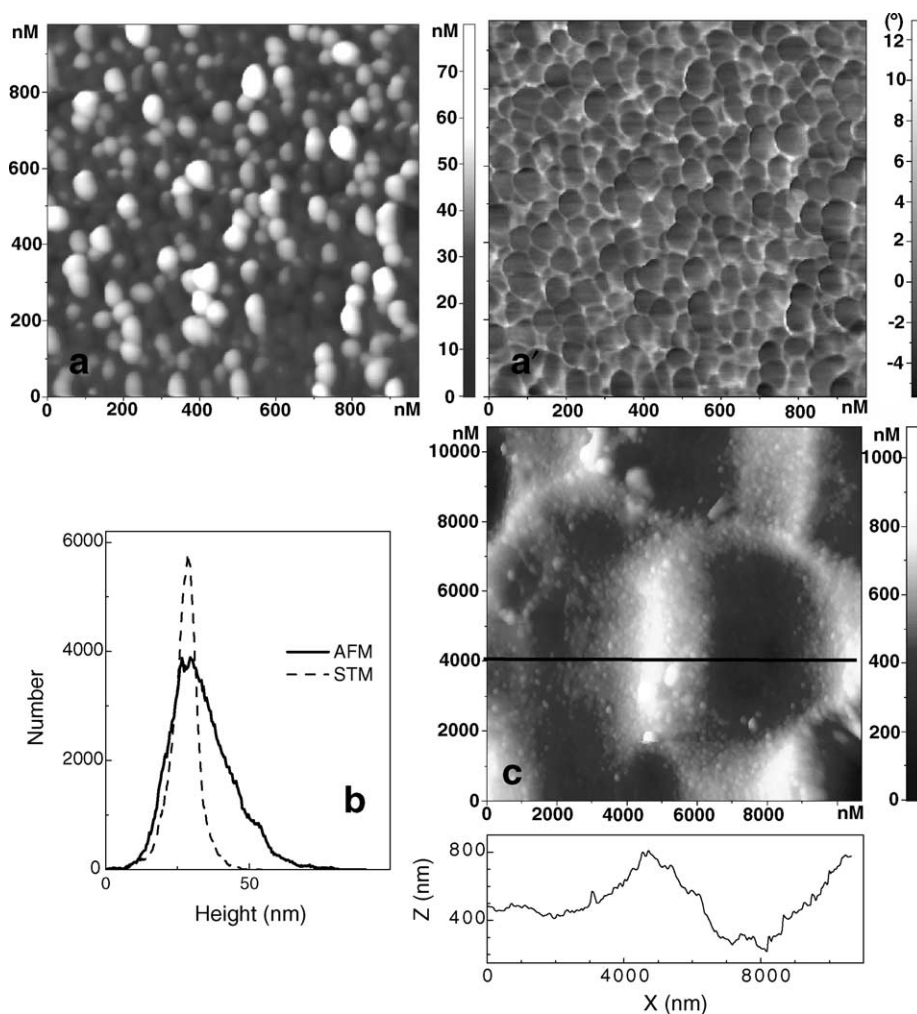


Fig. 4. Two-dimensional tapping-mode AFM images of PbS sample etched in 1 M HClO₄ at 50 °C for 1 h (a and a'—height and phase imaging), (b) typical histograms for the protrusion heights obtained from 1 $\mu\text{m} \times 1 \mu\text{m}$ AFM and STM images of the same sample. For the image (c) cross-sectional profile at $y = 4000 \text{ nm}$ is given.

The protrusions are about evenly distributed on the surface and overlap each other as well as the pit walls. The etching in 1 M HCl at the room temperature for 30 min (Fig. 5b) results in the surface morphology characterized by rare pits 50–100 nm in depth and two sorts of protrusions, with bigger ones being 100–300 nm in size and 20–30 nm high, while others being two to three times smaller and lower. De Guidici and Zuddas [32] observed similar surfaces of PbS interacted with more dilute HCl solutions at 20 °C for the time extended to 40 h; the authors believed that the protrusions are composed of elemental sulfur.

Wittstock et al. [29] also observed two types of sulfur deposits during anodic oxidation of galena in acetate buffer solution. In the current study, the protrusions exhibited considerable contrasts at the phase shift AFM images (Fig. 5b') and were also discerned using STM (not shown), so we doubt whether the protrusions are really composed of elemental sulfur or represent PbS irregularities, or, most likely, both of them, with thin S⁰ film covering the sulfidic phase projections. In all likelihood, the initial interaction of PbS with air-saturated acid solutions proceeds via both the non-oxidative mechanism releasing H₂S

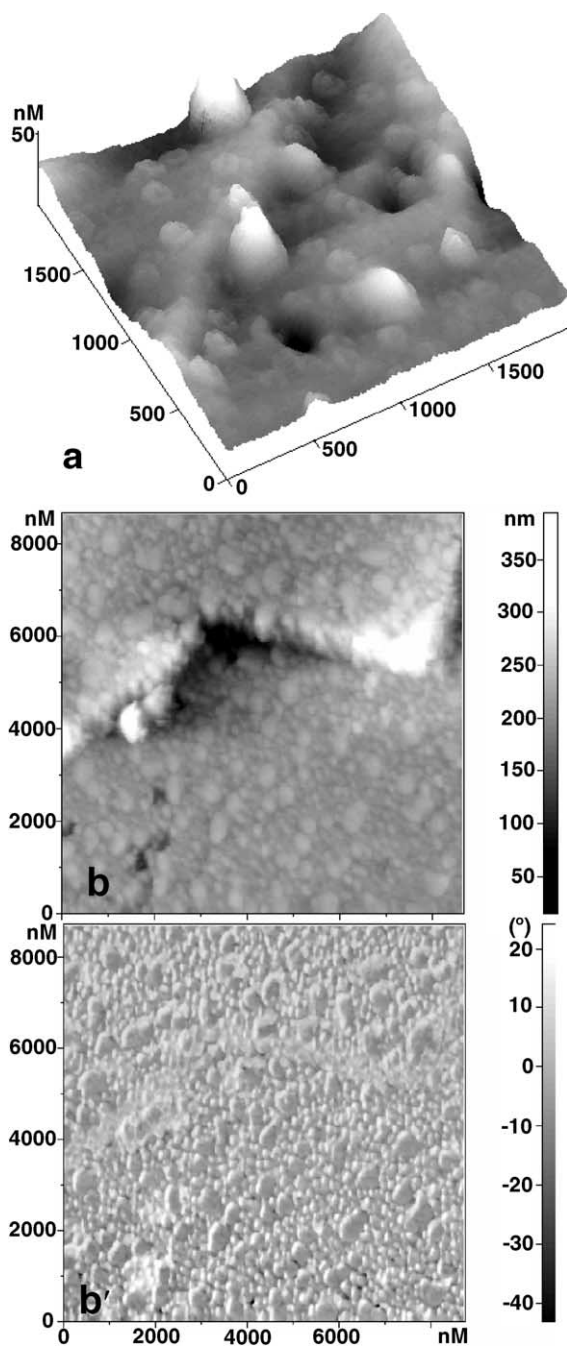


Fig. 5. Tapping mode AFM images of PbS etched in 1 M HCl at 20 °C for: (a) 15 min; (b) and (b') 30 min (height and phase imaging).

and forming the etch pits and the PbS or/and H₂S oxidation yielding S⁰, which may passivate the dissolution [32].

The PbS etching generally proceeds via the non-oxidative route at elevated temperatures [13] that results in enlargement of the pits up to several micrometers both in diameter and depth; the number of the lumps composed of other phases, probably elemental sulfur, diminishes (Fig. 6a–c). In contrast to perchloric acid, the etch pits have rounded shape and sharp edges, with the smaller pits often occurring at the bottom of larger ones. On certain stage, the features arrange for a ~10 μm “honeycomb” superstructure visible in SEM (Fig. 6e). The large-scale superstructure disappears with the etch progress, causing, especially at higher temperatures, effectively disordered surfaces with non-uniformly distributed deep pits (Fig. 6d). The surfaces treated at the elevated temperatures show also widespread 30–100 nm size protrusions of 10–50 nm in height, dimension and shape of which depend on the etch duration and temperature and their position relative to the pit walls. The phase imaging AFM, STM and STS show that the protrusions are created by the PbS material, but they apparently differ from those formed in perchloric acid media.

A series of experiments has been performed with HCl solutions containing small controlled concentrations of an oxidizing agent. It was found previously [12,13] that addition of 10⁻² to 10⁻⁵ M FeCl₃ effectively modified the dissolution kinetics and photoelectron spectra of the PbS surfaces, while retained the non-oxidative reaction mechanism. The PbS etching in 1 M HCl + 10⁻³ M FeCl₃ + 10⁻⁴ M NaI solutions (iodide-ions stabilize the reacted surfaces, playing, in particular, a role of a redox buffer [12,13]) at room temperatures produces 10–50 nm high protrusions of varying size and a small number of pits reaching 500 nm in diameter and 50 nm in depth (Fig. 7a). As the process moves on, the pits become imperceptible; big protrusions increase up to 1 μm in height and become fairly uniform in size and spatial distribution under certain conditions (Fig. 7b and c). In addition, fine structures formed by 30–200 nm details are present both on the protrusions and low areas (Fig. 7c). The dimensions of the relief features, which are certainly formed by PbS phase, gradually increase (Fig. 7d) until several

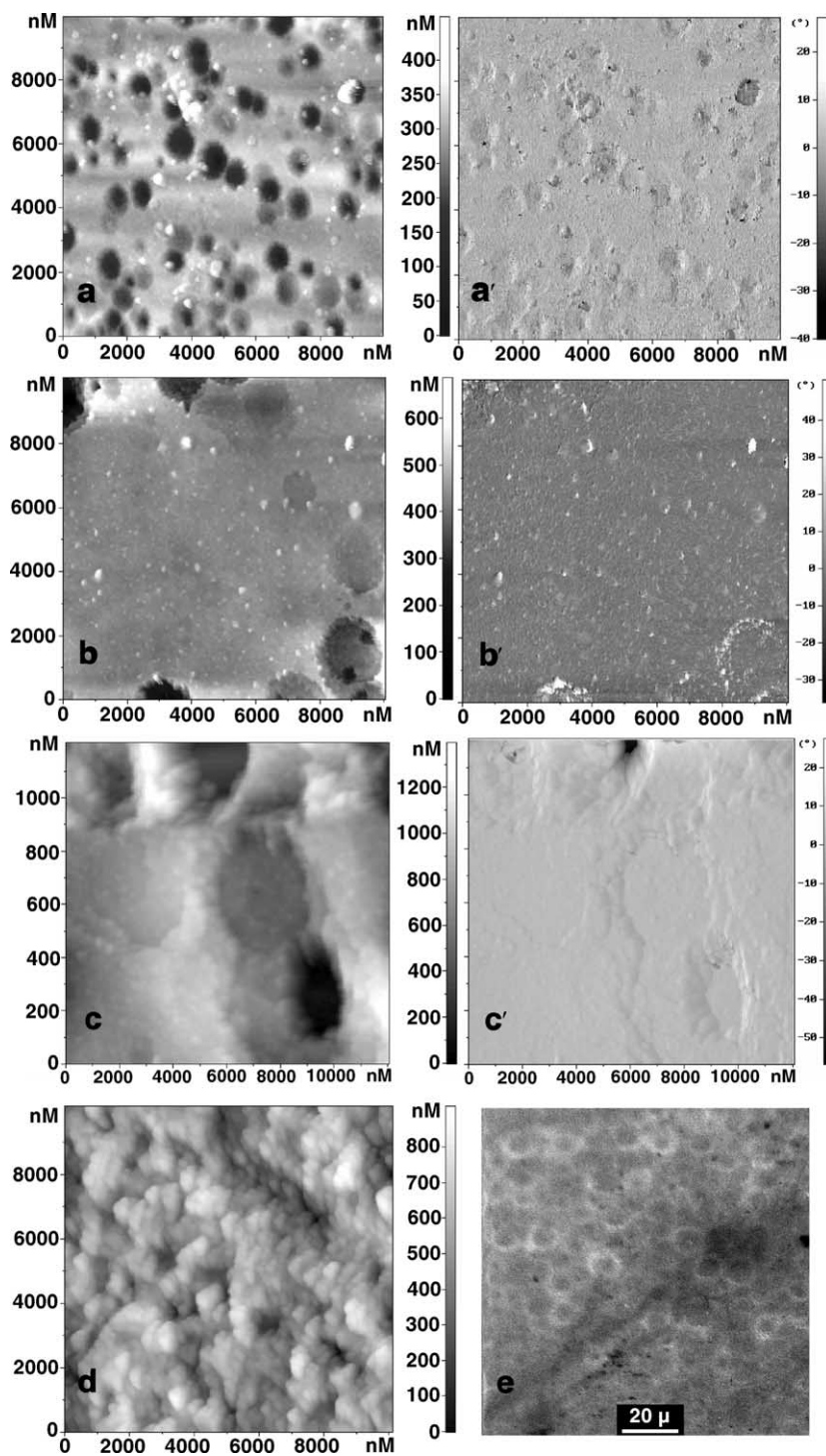


Fig. 6. Typical AFM images (height and phase imaging) of PbS surface etched in 1 M HCl: (a, a') at 30 °C for 30 min, (b, b') at 50 °C for 30 min, (c, c') at 50 °C for 60 min, (d) at 70 °C for 15 min. (e) SEM image of the PbS sample etched in 1 M HCl at 50 °C for 30 min.

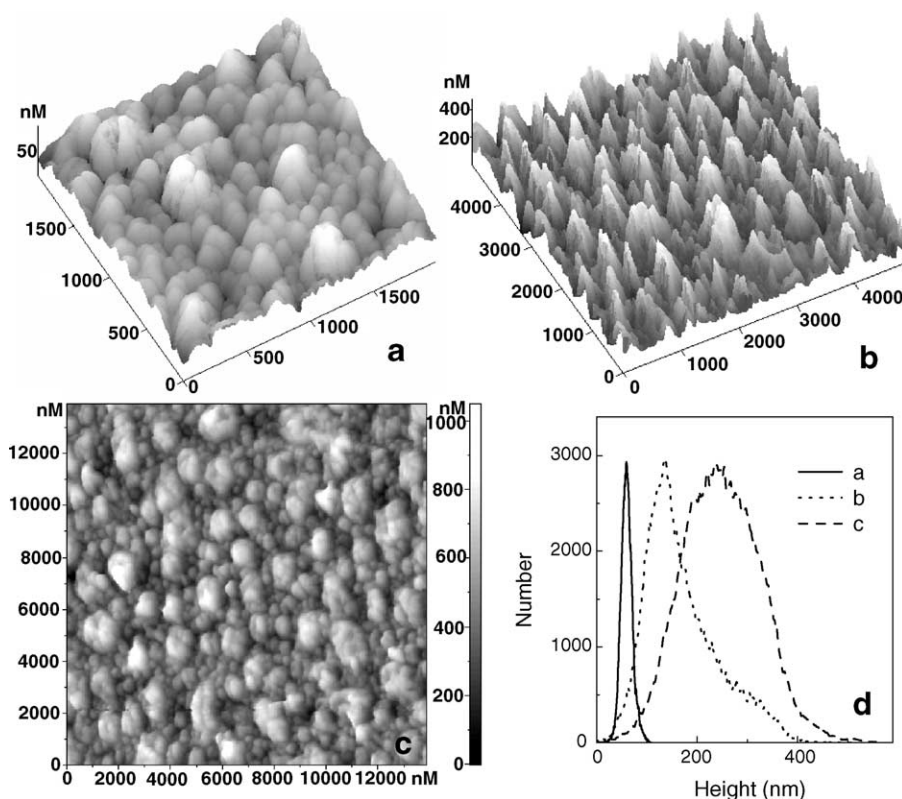


Fig. 7. PbS surfaces etched in 1 M HCl + 10^{-3} M FeCl₃ + 10^{-4} M NaI: (a) at 20 °C for 20 min, (b) at 50 °C for 10 min, and (c) at 50 °C for 30 min as imaged by STM (a) ($I = 0.1$ nA, $V = -0.1$ V) and tapping mode AFM (b and c). (d) Normalized histograms for the protrusion heights corresponding to the (a)–(c) images.

micrometer sized crystals, probably of lead iodide irretrievable by simple water rinsing, precipitate.

3.4. Tunneling spectra

Fig. 8 shows representative STS current–voltage data for the PbS (1 0 0) surfaces. The current versus sample voltage curves show a very low magnitude near the bias offset, indicating a conductance gap of about 0.4–0.5 eV, consistent with the bulk PbS characteristics [1,2]. The current increases at higher rate at negative voltages, suggesting an n-type semiconductor, only for samples fractured in air just in few minutes before the measurements, and such dependences were not observed at all in many cases. PbS ageing in air for several minutes or several hour results usually in quite symmetric I – V plots (as well as in dI/dV – V plots not shown in figures) which imply

rather a p- than n-type conductivity (Fig. 8a, 1) despite the bulk properties of the mineral. This is in well agreement with the n- to p-type conversion observed previously for thin films of $A^{II}B^{VI}$ and $A^{IV}B^{VI}$ compounds exposed to oxygen (e.g. [34]) and for natural PbS crystals cleaved under an aqueous 0.1 M sodium tetraborate solution [35]. The phenomenon was interpreted using models, which suggested at first the adsorption of oxygen tying free electrons or/and bonding interstitial Pb ions (donors) and then the formation of acceptor-like vacancies of lead in the surface layer. After the contact of lead sulfide with atmosphere for several days and longer, the tunneling current noticeably decreases at positive sample biases (Fig. 8a, 2), implying emergence of a new sort of donor-like defects on the extensively oxidized PbS surfaces, which possible nature is discussed in detail below.

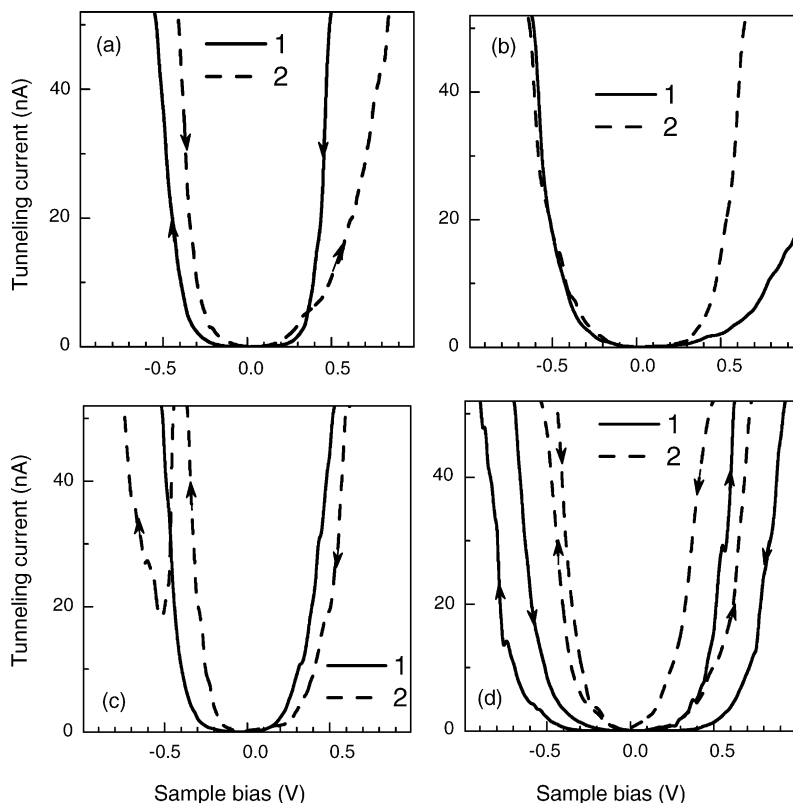


Fig. 8. Tunneling spectra of PbS (1 0 0) surfaces: (a) exposed at atmosphere for 1 h (1) and 1 month (2), (b) etched in 1 M HClO₄ at 50 °C for 20 min (1) and at 50 °C for 1 h (2), (c) etched in 1 M HCl at 50 °C for 1 h at terraces between the etch pits (1) and at the bottom of the pits (2), (d) etched in 1 M HCl + 10⁻³ M FeCl₃ + 10⁻⁴ M NaI at 20 °C for 20 min (1) and at 50 °C for 30 min (2).

STS plots given in Fig. 8b demonstrate that the surface formed at the initial stages of the perchloric acid etching exhibits clear n-type conductivity, and the samples produced by longer treatment typically show weak n-type conductivity, indicating the formation of donor-type defects due to the chemical treatment.

Tunneling spectra I - V acquired on various PbS surfaces treated in HCl solutions (Fig. 8c) usually suggest p-type conductivity. The plots associated with the etch pit bottoms, especially for the surfaces obtained under more reductive conditions (in deoxygenated solutions or in the presence of PbS powder), often show peaks at the I - V and dI/dV plots going in the negative direction (e.g., from +1 to -1 V) at the negative potentials from -0.1 to -0.3 V. Such kind of the spectra was well reproduced, as a rule, within 50–

100 nm areas. The peaks can be assigned to very large density of electronic gap states below the Fermi level, which have high electron affinity, i.e. acceptors.

The I - V plots measured in the hydrochloric acid with Fe³⁺ and I⁻ added notably depend on the direction of the bias voltage sweep (Fig. 8d). The etching at 20 °C results in about symmetric curves suggesting slightly p-type conductivity, with the plots obtained in the negative-going potential sweep being somewhat wider. This may be rationalized in terms of both donor and acceptor gap levels and the Fermi level pinned in the middle of the gap of the reacted surface layer, akin to a compensated semiconductor. The asymmetry and different shifts of the spectra are evident for the samples etched at higher temperatures; the positive-going plots indicate usually n-type while the negative-going ones show obvious p-type surfaces.

Tunneling spectra differ on various surface spots, although we failed to establish reliable regularities between the relief features and the STS characteristics, except for trivial increase in the tunneling currents near steep topographic slopes. The STS plots depend also on the potential sweep rate; this phenomenon related with impedance measurements, as well as spatially resolved characteristics and the effect of voltage sweep direction are worth further examination.

4. Discussion

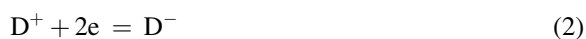
4.1. Nature of heterogeneity and defects

While inherent defects in original PbS are most likely responsible for the spatially non-uniform corrosion of the material at initial stages [25–31], the results of the current study suggest that the surface heterogeneity formed over the prolonged oxidation or etching is mainly due to defects generated by chemical reactions. As far back as in late 1950s, Plaksin and co-workers [36] attributed the effect of oxygen on the flotation of galena to the formation of acceptor-type cation vacancies via the reaction



This hypothesis was later supported by direct measurements of semiconducting characteristics of the oxidized PbS [34,35] and XPS studies [4,9–14], which often found the surface depletion in lead over sulfur beyond the stoichiometry range of the PbS compound. Furthermore, photoemission spectra of the valence band and X-ray spectroscopy demonstrated distortions of chemical bonding in the acid reacted, non-stoichiometric layers [12,13], and the above STS findings suggest a complicated behavior of defect centers rather than the straightforward formation of acceptor gap states by lead vacancies.

It was previously proposed [8,12,13,37,38] to consider the modified, disordered surface layers of metal sulfides similar to non-crystalline semiconductors [15,16], using, in particular, the concept of centers D^+/D^- having negative correlation energy. These centers convert one into another when charged



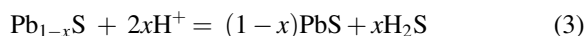
exhibiting a series of electronic levels in the gap, energy positions and relative densities of which depend upon both the Fermi level position and the rates of the atomic rearrangement after the charge transfer, with states occupied by one electron being unstable [15,16]. The mobility of normally octahedrally coordinated S and Pb atoms is thought to remain comparably low in the metal deficient surface layers, so centers D^+ and D^- can have non-equilibrium, considerably different concentrations [8,12,13]. These characteristics are affected by composition and structure of the altered layers and so by reaction conditions. In particular, the sort of acid anion has dramatic effect on the dissolution kinetics and the reaction layer of PbS, probably via properties of surface Pb–anion complexes and the rate of metal release [12,13].

From this standpoint, tunneling spectra obtained in the present research during the long-term exposure of PbS to atmosphere imply the formation first of acceptor-like D^- centers, in agreement with the previous work [34,35], and then of prevailing D^+ -type centers. Initial, room temperature etching in 1 M HClO_4 produces clear n-type conductivity and hence D^+ defects, a part of which disappear or transform into D^- at later etch stages. The hydrochloric acid treatment entails the preferential formation of acceptors D^- . The I – V curves measured at the surfaces conditioned in hydrochloric acid solutions with ferric iron and iodide ions added have complex character that may be explained by the presence of both sorts of defects and their slow mutual conversion, although this requires further examination. These conclusions coincide in the main with those derived from spectroscopic studies on the sample treated in the same solutions [12].

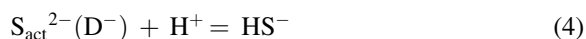
4.2. Dissolution mechanisms

The PbS dissolution at room temperature and elevated temperatures, excepting possibly in the $\text{HCl} + \text{FeCl}_3 + \text{NaI}$ electrolyte, appear to proceed via various mechanisms. The difference may be assigned to more oxidative media at the lower temperature owing to higher concentration of dissolved oxygen. Preliminary oxidation of PbS in air plays a role at the early stage of the etching too. As a result, some surface areas dissolve at very low rate because of passivation by elemental sulfur or special

properties of the sulfidic phase. Composition of aqueous solutions was not monitored in this study, but the SPM and STS experiments can be compared with the kinetics of rotating PbS disk dissolution [13,39]. The macroscopic dissolution rate increases in the range $1 \text{ M HClO}_4 < 1 \text{ M HCl} < 1 \text{ M HCl} + 0.001 \text{ M FeCl}_3 + 10^{-4} \text{ M NaI}$ at 50°C ; the kinetic parameters are dependent on the acid media composition as well [13]. In all cases the reaction order with respect to hydrogen ion activity lays between 0.5–0.6 and 1, implying that the process is controlled mostly by the interaction of H^+ ions with a sulfur species [13,37,39,40]. The real surfaces of metal sulfides are commonly metal-deficient, so the preferential release of metals (Eq. (1)) seems to represent a first step of the process, and the active S species are associated with S atoms neighboring metal vacancies



We assume that the D^- -type centers, which are thought to comprise under-coordinated chalcogen atoms having increased negative charge as compared with regular anionic sites [12,15,16], are involved in reaction (3), yielding HS^- in the rate-limiting step



and then H_2S as the end product. Indeed, one can see a correlation between the macroscopic rates of the non-oxidative dissolution and the surface-averaged contents of acceptors and, especially, the one between the fast local dissolution producing the deep etch pits and the large densities of the D^- centers at the pit bottoms for PbS etched in 1 M HCl at elevated temperatures. The surface morphologies imply that the process is in fact self-catalytic, in conformity with somewhat sigmoid kinetic curves [13]. It is also likely that p-type regions oxidize faster than n-type surfaces. On the contrary, the surfaces enriched by donor-like defects are believed to be inactive both in the non-oxidative dissolution and oxidation [8,13,37,38]. This suggests that the D^+ centers should convert into D^- centers before the interaction with H^+ ions. If the transformation (Eq. (2)) approaches quasi-equilibrium, it is governed by the Fermi level energy, that is the D^- concentration increases with decreasing the electrochemical potential of PbS. At low electrode potentials, however, this concentration is limited by the rate, but

not the equilibrium, of the D^+ to D^- transition or by the metal release rate (Eq. (1)), so the dissolution rate as a function of electrode potential shows a maximum [13].

4.3. Surface patterning

It is commonly accepted that both heavily doped crystalline semiconductors and non-crystalline ones have geometrically inhomogeneous distribution of defect densities, resulting in large-scale electrostatic potential fluctuations and rather small deformation fluctuations related to the distortions of chemical bonding [15,16]. The heterogeneity of the reacted surfaces is not, however, entirely stochastic but obeys the regularities linked with the reaction kinetics and mechanisms, suggesting that the major factors responsible for self-organization and patterning of the surfaces are local contents of D^+ and D^- defects, varying over the process. It is worth mentioning that these centers transform one into another by reaction (2) when the Fermi level shifts or concentration of a center increases above a threshold [12].

The fluctuations of potential and dissolution rate are small if the Fermi level is pinned by the two levels of D^+ and D^- centers in the gap middle akin to chalcogenide glasses [16] or/and predominating D^+ centers retard the dissolution at active spots. Relatively smooth surfaces formed under these circumstances show primarily nano-scale relief features, which are attributable to the stochastic deformation fluctuations; this seems to be the case for the PbS etched in HClO_4 solutions. The submicrometer-sized topography features produced in the $\text{HCl} + \text{Fe}^{3+}$ solutions appear to be due to a co-existence of areas with predominant D^- and D^+ or D^+/D^- centers. This causes big differences in local positions of the Fermi level, resembling the electrostatic potential fluctuations, and effectively distinct local dissolution rates. These variations in the Fermi level energy are consistent with the very broad S 2p and Pb 4f lines in photoelectron spectra obtained from such a surface [12].

The tailoring of metal sulfide surfaces by the simple etch procedure that fabricates simultaneously nano- and micrometer-scale topographic features, well-ordered at certain stages, may be of interest for such applications of PbS and related materials as IR-

detectors and sensors. Further research is necessary in order to understand better the mechanisms of both the dissolution and solid state reactions, and to work out techniques forming predetermined patterns.

5. Conclusions

The exposure of PbS to atmosphere at high relative humidity produces protrusions of about 20 nm in size, which evenly cover the surface after 3–5 days and then coalesce; the protrusions composed of loose oxidation products do not arise at low RH. Therefore, water condensed on the surface promotes the PbS oxidation and wets and renders the products. The tunneling current versus sample bias plots suggest n- to p-type and then p- to n-type inversion of the surface conductivity during the aerial oxidation. The etching of PbS in 1 M HClO₄ creates the protrusions of the sulfide phase of 20–80 nm in size and the shallow valleys of several micrometers in length; the reacted surfaces exhibit clear n-type conductivity at initial stages and typically show weak n-type after the treatment at temperatures above 30 °C. The surfaces etched in 1 M HCl at room temperature become covered by low protrusions mostly less than 100 nm in diameter along with square and rounded pits less 50 nm deep. The etch pits up to few micrometers in diameter and in depth and a honeycomb structure of about 10 μm in size arise along with less than 100 nm relief features at the elevated temperatures. The tunneling spectra are indicative of p-type conductivity; the plots associated with the etch pits often show peaks at negative sample biases due to a large density of acceptor states. Hydrochloric acid solutions containing 10⁻³ to 10⁻⁴ M FeCl₃ and NaI produce the surface topography constructed by rather uniformly distributed large PbS protrusions, growing up to ~1 μm with the etching progress, together with smaller details. STM and STS data confirm that these features are formed by PbS phase but not elemental sulfur or other reaction products. The changes in topography and semiconducting properties of PbS are considered to be due to the non-uniform distribution and self-organization of chemically induced defect centers, which determine the local rates of PbS corrosion. The complicated behavior of the centers can be explained in terms of their negative correlation

energy (Hubbard energy), by analogy with the non-crystalline semiconducting chalcogenides.

Acknowledgement

This work was supported in part by the Russian Foundation for Basic Research, project 01-03-32687a.

References

- [1] J.A. Tossell, D.J. Vaughan, *Can. Mineral.* 25 (1987) 381.
- [2] T. Okuno, A.A. Lipovskii, T. Ogawa, I. Amagai, Y. Masumoto, *J. Lumin.* 87–89 (2000) 491.
- [3] S. Evans, E. Raftery, *J. Chem. Soc., Faraday Trans. I* 78 (1982) 3545.
- [4] A.N. Buckley, R. Woods, *Appl. Surf. Sci.* 17 (1984) 401.
- [5] D. Fornasiero, F.S. Li, J. Ralston, R.S.C. Smart, *J. Colloid Interf. Sci.* 164 (1994) 333.
- [6] P. Novak, K. Laajalehto, *Appl. Surf. Sci.* 157 (2000) 101; P. Novak, K. Laajalehto, I. Kartio, *Colloids Surf. A* 161 (2000) 447.
- [7] I.V. Chernyshova, *J. Phys. Chem. B* 105 (2001) 8178.
- [8] Yu. L. Mikhlin, A. Kuklinskiy, E. Mikhlina, V. Kargin, I. Asanov, *J. Appl. Electrochem.* 34 (2004) 37.
- [9] I. Kartio, K. Laajalehto, T. Kaurila, E.J. Suoninen, *Appl. Surf. Sci.* 93 (1996) 167.
- [10] A.N. Buckley, R. Woods, *J. Appl. Electrochem.* 26 (1996) 899.
- [11] I. Kartio, K. Laajalehto, E.J. Suoninen, A.N. Buckley, R. Woods, *Colloids Surf. A* 133 (1998) 303.
- [12] Yu.L. Mikhlin, Ye.V. Tomashevich, I.P. Asanov, A.V. Okotrub, *Poverkhnost. Rentgen. Neitron. Synhrotron. Issled.* 12 (1998) 77.
- [13] Yu. Mikhlin, Ye. Tomashevich, I. Asanov, A. Okotrub, in: R. Woods, F.M. Doyle (Eds.), *Electrochem. Mineral. Metal Process. V*, vol. 14, The Electrochem. Soc. Proc. Ser., Pennington, NJ, 2000, p. 282.
- [14] R.S. Smart, W.M. Skinner, A.R. Gerson, *Surf. Interf. Anal.* 28 (1999) 101.
- [15] N.F. Mott, E.A. Davis, *Electron Processes in Non-Crystalline Materials*, Clarendon Press, Oxford, 1979.
- [16] K.D. Tsandin (Ed.), *Electron Phenomena in Chalcogenide Glassy Semiconductors*, Nauka, St. Petersburg, 1996.
- [17] C.M. Eggleston, M.F. Hochella Jr., *Geochim. Cosmochim. Acta* 54 (1990) 1511.
- [18] C.M. Eggleston, M.F. Hochella Jr., *Science* 254 (1991) 983.
- [19] C.M. Eggleston, M.F. Hochella Jr., *Am. Mineral.* 78 (1993) 877.
- [20] C.M. Eggleston, M.F. Hochella Jr., *Environmental geochemistry of sulfide oxidation*, ACS Symp. Ser. 550 (1994) 201.
- [21] C.M. Eggleston, *Geochim. Cosmochim. Acta* 61 (1997) 657.
- [22] U. Becker, M.F. Hochella Jr., *Geochim. Cosmochim. Acta* 60 (1996) 2413.

- [23] U. Becker, D.J. Vaughan, M.F. Hochella Jr., *Geochim. Cosmochim. Acta* 61 (1997) 3565.
- [24] U. Becker, S.P. Greatbanks, K.M. Rosso, I.H. Hillier, D.J. Vaughan, *J. Chem. Phys.* 107 (1997) 7537.
- [25] K. Laajalehto, R.St.C. Smart, J. Ralston, E. Suoninen, *Appl. Surf. Sci.* 64 (1993) 29.
- [26] B.S. Kim, R.A. Hayes, C.A. Prestige, J. Ralston, R.S.C. Smart, *Appl. Surf. Sci.* 78 (1994) 385.
- [27] B.S. Kim, R.A. Hayes, C.A. Prestige, J. Ralston, R.S.C. Smart, *Langmuir* 11 (1995) 2554.
- [28] B.S. Kim, R.A. Hayes, C.A. Prestige, J. Ralston, R.St.C. Smart, *Colloids Surf. A* 117 (1996) 117.
- [29] G. Wittstock, I. Kartio, D. Hirsch, S. Kunze, R. Szargan, *Langmuir* 12 (1996) 5709.
- [30] S.R. Higgins, R.J. Hamers, *Surf. Sci.* 324 (1995) 263.
- [31] S.R. Higgins, R.J. Hamers, *Geochim. Cosmochim. Acta* 60 (1996) 2789.
- [32] G. De Giudici, P. Zuddas, *Geochim. Cosmochim. Acta* 65 (2001) 1381.
- [33] J. Cama, P. Acero, C. Ayora, A. Lobo, *Chem. Geol.* 214 (2005) 309.
- [34] E.H.C. Parker, D. Williams, *Thin Solid Films* 35 (1976) 373.
- [35] P.E. Richardson, C.S. O'Dell, *J. Electrochem. Soc.* 132 (1985) 1350.
- [36] I.N. Plaksin, *Trans. AIME* 214 (1959) 319;
I.N. Plaksin, R.Sh. Shafeev, *Trans. Inst. Min. Metall.* 72 (1963) 715.
- [37] Yu. Mikhlin, *Phys. Chem. Chem. Phys.* 2 (2000) 5672.
- [38] Yu.L. Mikhlin, Ye.V. Tomashevich, I.P. Asanov, A.V. Okotrub, V.A. Varnek, D.V. Vyalikh, *Appl. Surf. Sci.* 225 (2004) 395.
- [39] Y. Awakura, S. Kamei, H. Majima, *Metall. Trans. B* 11 (1980) 377.
- [40] A.R. Gerson, A.R. O'Dea, *Geochim. Cosmochim. Acta* 67 (2003) 813.